6-28-2022

Time-varying resonant mass at collider and beam dump experiments

Jinhui Guo

Yuxuan He

Jia Liu

Xiao-Ping Wang

Ke-Pan Xie

Time-varying resonant mass at collider and beam dump experiments

Jinhui Guo,[1,*] Yuxuan He,[1,†] Jia Liu,[1,2,‡] Xiao-Ping Wang,[3,4,§] and Ke-Pan Xie[5,¶]

[1] *School of Physics and State Key Laboratory of Nuclear Physics and Technology, Peking University, Beijing 100871, China*
[2] *Center for High Energy Physics, Peking University, Beijing 100871, China*
[3] *School of Physics, Beihang University, Beijing 100083, China*
[4] *Beijing Key Laboratory of Advanced Nuclear Materials and Physics, Beihang University, Beijing 100191, China*
[5] *Department of Physics and Astronomy, University of Nebraska, Lincoln, NE 68588, USA*

A new particle usually manifests itself as a single resonant peak located at its mass. We propose if the new particle mass is time-varying due to environmental effects, then its mass spectrum typically has a novel double-peak feature. A representative model is the kinetic mixing dark photon interacting with an ultralight complex scalar dark matter charged under $U(1)'$. We reanalyze the existing experiments, showing the constraints on such a model are drastically weakened than those on the traditional single-peak resonance model, due to the reduction of the luminosity exposure in each resonant mass bin. Consequently, for mass around tens of MeV, the muon g_μ–2 solution from the kinetic mixing dark photon becomes viable again. The scenario can be further tested by reanalyzing the existing data with timing information included.

I. INTRODUCTION

The idea of varying fundamental constants can be traced back to the 1930s from Dirac [1], whereas more contemporary literature predicts variations of the fine structure constant, nucleon mass, electron-to-proton mass ratio, gauge, and gravity couplings at cosmological time scale [2–5]. Recently, people proposed those time-varying fundamental constants could originate from ultralight bosonic dark matter (DM) [6–8]. It can induce time oscillation in Standard Model (SM) gauge couplings and fermion masses, where the variation period is related to the DM mass [9–11]. Transient temporal changes can also be induced by topological DM [12–14]. Such scenarios can be probed in atomic, molecular, and optical physics, Oklo phenomenon and astrophysical experiments [5, 15, 16].

While previous literature mainly considers the time-varying effects of SM couplings and masses in low energy experiments, in this *work*, we consider the time oscillation of the dark sector particle mass and its implication at high energy colliders and beam dump experiments. In general, it can reduce the luminosity exposure in each resonant mass bin, changing the experimental constraints drastically. Furthermore, the invariant mass spectrum has the multi-peak (typically double-peak) feature rather than the traditional single-peak feature.

The illustrative example is the kinetic mixing dark photon model [17–19] mediating the SM and dark sector with mixing strength ϵ [6, 20–23]. Particle experiments have placed stringent bounds on ϵ and mass $m_{A'}$ [24, 25]. In particular, the parameter space explaining the recent muon $(g-2)_\mu$ excess [26, 27] has been ruled out [25, 28]. However, we show that, if there is an ultralight scalar DM ϕ charged under the dark $U(1)'$, then it can induce a periodic oscillation of A' mass. It significantly weakens the existing collider and beam dump bounds, especially the resonance of dilepton searches [29–34], that even the highly excluded dark photon solution to muon g_μ–2 becomes viable again. Moreover, we propose using the time information of the recorded events, which can place more stringent limits on the signal and is possible to pull out the oscillation period if the signal does exist. Our analysis can apply similarly to other dark mediators.

II. TIME-VARYING MASS OF THE PARTICLE

We assume the resonant particle has a time dependent mass $m_{\rm res}(t)$ due to environmental effects, and further take a time oscillating form with period of τ,

$$m^2_{\rm res}(t) = m^2_{\rm res}(t+\tau). \tag{1}$$

For the resonant searches, the invariant mass of the event changes with time, thus the strategy of looking for resonance in a fixed bin suffers from the reduced time exposure in that bin and the leakage into other bins. If the data taking time $t_{\rm exp} \gg \tau$ and the experiment analyzes the full data in a time-blind way, then the relevant physical quantity is the time exposure Δt_i in the ith mass bin $[m_i, m_{i+1}]$, with the expression

$$\Delta t_i = \frac{t_{\rm exp}}{\tau}\int_{m_i}^{m_{i+1}} \left|\frac{dt}{dm_{\rm res}}\right| dm_{\rm res}. \tag{2}$$

Instead of a narrow resonance, the signal has a spread template fully determined by $dt/dm_{\rm res}$. Then, the event number in ith bin is

$$N_i = \sigma^{(i)}_{\rm res}\epsilon_i {\rm L}\frac{\Delta t_i}{t_{\rm exp}}, \tag{3}$$

where $\sigma^{(i)}_{\rm res}$ and ϵ_i are the resonant production cross-section and cut-efficiency for ith bin, respectively, while

* guojh23@pku.edu.cn
† heyx25@pku.edu.cn
‡ jialiu@pku.edu.cn
§ hcwangxiaoping@buaa.edu.cn
¶ kepan.xie@unl.edu

L is the total luminosity. Since the particle production and decay happen very quickly, the resonant mass is unchanged in a single event. Therefore, the difference between our analysis and the previous resonant analysis is fully described by the time exposure fraction $\Delta t_i/t_{\rm exp}$.

There is a *double-peak* feature in the time-varying mass scenario that the peaks must show up at the minimum and maximum of resonant mass. Assuming the function $m_{\rm res}(t)$ is continuous and differentiable, the physical mass exists global minimum and maximum regardless of its periodic feature. Thus, it must have $dm_{\rm res}/dt = 0$ at two extreme points and the time exposure blows up accordingly. Additional local extrema can also contribute to peaks, leading to the multi-peak scenario.

III. MODEL SETUP

We consider a kinetic mixing dark photon A' with $U(1)'$ interaction,

$$\mathcal{L} = -\frac{1}{4}F'_{\mu\nu}F'^{\mu\nu} + \frac{1}{2}m_0^2 A'_\mu A'^\mu + \epsilon e A'_\mu J^\mu_{\rm em}, \tag{4}$$

where ϵ is the kinetic mixing strength which controls the strength of A' coupling to electromagnetic current $J_{\rm em}$. The mass m_0 is a constant from $U(1)'$ spontaneously breaking. In addition, we consider a complex scalar DM ϕ with small charge Q_ϕ under $U(1)'$. The ultralight scalar DM obtains its relic abundance through misalignment mechanism [35–38], satisfying the equation of motion

$$\ddot{\phi} + 3H\dot{\phi} + m_\phi^2\phi = 0, \tag{5}$$

and at late time it is locally described by the classical wave function $\phi(t)$,

$$\phi(t) \approx \phi_1 \cos(m_\phi t) + \phi_2 \sin(m_\phi t), \tag{6}$$

where $\phi_{1,2}$ are the complex field strengths, satisfying $\rho_{\rm DM} \approx \left(|\phi_1|^2 + |\phi_2|^2\right) m_\phi^2$ in the non-relativistic limit. In the scalar quantum electrodynamics (QED), one can have the following four-point vertex

$$\left(D_\mu\phi\right)^* D^\mu\phi \supset \left(g'Q_\phi\right)^2 \phi^*\phi A'_\mu A'^\mu. \tag{7}$$

It effectively leads to time oscillating A' mass today as

$$m_{A'}^2(t) = \tilde{m}_0^2\left(1 + \kappa\cos^2\left(m_\phi t\right)\right), \tag{8}$$

$$\tilde{m}_0^2 = m_0^2 + \left(g'Q_\phi\right)^2\left(\phi_1^*\phi_1 + \phi_2^*\phi_2 - \sqrt{x^2+y^2}\right), \tag{9}$$

$$\kappa \equiv 2(g'Q_\phi)^2\sqrt{x^2+y^2}/\tilde{m}_0^2, \tag{10}$$

where κ is the amplitude of the oscillation, $x = |\phi_1|^2 - |\phi_2|^2$ and $y = \phi_1\phi_2^* + \phi_1^*\phi_2$. Thus, the oscillation mass is fully determined by three parameters, $\tilde{m}_0$, κ and m_ϕ, with the phase removed by the definition of $t = 0$.

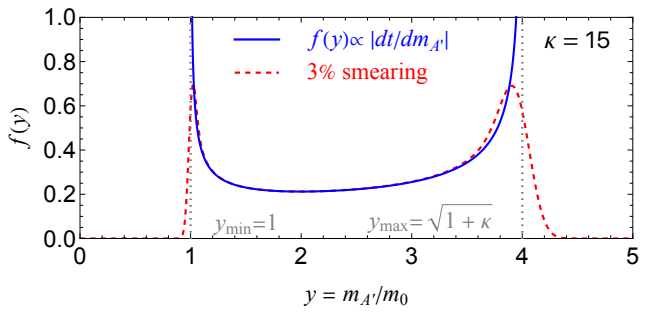

Figure 1. The normalized PDF $f(y)$ before and after smearing with a detector resolution of 3%.

The mass ratio $y(t) \equiv m_{A'}(t)/\tilde{m}_0$ has minimum $y_{\rm min} = 1$ and maximum $y_{\rm max} = \sqrt{1+\kappa}$ respectively, and oscillates with time period of $\tau \equiv \pi/m_\phi$. From Eq. (2), the invariant mass bin has a time exposure proportional to

$$\left|\frac{dt}{dm_{A'}}\right| = \frac{\tau}{m_0} f(y), \tag{11}$$

where a factor of 2 is multiplied since each mass appears twice in one period. The probability density function (PDF),

$$f(y) = \frac{2y}{\pi\sqrt{\left(y^2 - y_{\rm min}^2\right)\left(y_{\rm max}^2 - y^2\right)}}, \tag{12}$$

is normalized between $y \in [y_{\rm min},\ y_{\rm max}]$. Indeed, the time exposure diverges at the minimum and maximum of the resonant mass bin in Fig. 1. After including the detector resolution, it becomes finite and shows the *double-peak* feature. The right peak contains larger probability than the left one, because $f(y) \propto y$. One can evaluate the probability difference contained in the two peaks,

$$\frac{\int_{y_{\rm max}-\Delta}^{y_{\rm max}} f(y)dy}{\int_{y_{\rm min}}^{y_{\rm min}+\Delta} f(y)dy} \xrightarrow{\Delta\to 0} \sqrt{\frac{y_{\rm max}}{y_{\rm min}}}, \tag{13}$$

which is a factor of 2 difference for $\kappa \sim \mathcal{O}(15)$.

If the data taking duration lasts much longer than the oscillation period, $t_{\rm exp} \gg \tau$, the events will run between $\tilde{m}_0$ and $\sqrt{1+\kappa}\tilde{m}_0$ many times. In this case, the normalized mass spectrum $f(y)$ fully describes the data distribution, without explicit dependence on t, initial oscillation phase, or m_ϕ. Since Lyman-alpha constraints require $m_\phi \gtrsim 2\times 10^{-20}$ eV [39] suggesting longest oscillation period of about one day, most of the experiments satisfy the $t_{\rm exp} \gg \tau$ condition.

For simple connection to ultraviolet complete model parameters, we assume $\arg[\phi_1] = \arg[\phi_2]$ or $\phi_2 = 0$ to have

$$\tilde{m}_0 = m_0, \quad \kappa \equiv 2(g'Q_\phi)^2\rho_{\rm DM}/\left(m_\phi^2 m_0^2\right). \tag{14}$$

Moreover, we are interested in parameter space $m_0 \sim \mathcal{O}(0.1)$ GeV and $\kappa \sim \mathcal{O}(10)$, connecting to luminosity

Collaboration	Production mode	Experimental environment	Spectrum	Resolution $\sigma_{\rm re}$	Fit window	Range of $m_{A'}$
BaBar [29]	$e^+e^- \to \gamma A'$	$\sqrt{s} \approx 10$ GeV, 514 fb^{-1}	m_{ee}, $m_{\mu\mu}$	[1.5, 8] MeV	$m_{A'} \pm 10\,\sigma_{\rm re}$	[0.02, 10.2] GeV
LHCb [30–32]	$pp \to A'$	$\sqrt{s} = 13$ TeV, ~ 5 fb^{-1}	$m_{\mu\mu}$	[0.12, 380] MeV	$m_{A'} \pm 12.5\,\sigma_{\rm re}$	[0.214, 69.8] GeV
A1 [33]	$e^- Z \to e^- Z A'$	$E_e \in [0.180, 0.855]$ GeV	m_{ee}	0.5 MeV	$m_{A'} \pm 3\,\sigma_{\rm re}$	[0.040, 0.300] GeV
NA48/2 [34]	$\pi^0 \to \gamma A'$	1.69×10^7 $\pi^0 \to \gamma e^+ e^-$ events	m_{ee}	[0.16, 1.33] MeV	single bin	[0.009, 0.120] GeV

Table I. The summary table for experiments using the dilepton resonance to search for A'.

frontier experiments. Normally, the dark photon A' with muon coupling can contribute to $(g-2)_\mu$ as $\Delta a_\mu(m_{A'})$. In the time-varying mass scenario, one should average over time as

$$\frac{1}{\tau}\int_0^\tau dt\ \Delta a_\mu\left(m_{A'}(t)\right). \tag{15}$$

Since the varying mass is larger than m_0, it generally needs larger ϵ to explain the muon $(g-2)_\mu$ anomaly. In addition, the limit from $(g-2)_e$, $\Delta a_e < 0.98 \times 10^{-12}$ at 95% C.L. [40], can also be used to constrain the scenario.

IV. RECASTING VIA THE DOUBLE-PEAK METHOD

The dark photon has been searched for in the dilepton channels $A' \to \ell^+\ell^-$ ($\ell = e,\ \mu$) with various production mechanisms [29–34]. The general strategy is to fit the dilepton invariant mass spectrum $m_{\ell\ell}$ with a given signal hypothesis in a mass window broader than a few times of the energy resolution $\sigma_{\rm re}$. The upper limits on the production cross section can be translated into bounds on ϵ^2 as a function of $m_{A'}$. For a given mass window, we fit the $m_{\ell\ell}$ spectrum with a quadratic or cubic function and compare it to the observed data with and without the signal events to get the likelihoods $\mathcal{L}$ and $\mathcal{L}_0$, respectively. Then we require the log-likelihood ratio (LLR) $\mathcal{S} \equiv -2\ln(\mathcal{L}/\mathcal{L}_0) = 3.84$, to obtain the upper limit for signal event number [41].

We first recast the traditional single-peak resonance signal method for dilepton experiments following the experimental setups summarized in Table I. Our recast results agree with the experimental results quite well, and the calculations and methods are detailed in the Appendix [25, 29, 31–33, 42–47]. We next apply our time-varying resonance signal model to fit the background data. According to the *double-peak* feature of the signal, for a fixed mass window centering around $m_{A'}$, there are two signal peaks to fit, the minimum $m_{A'} = m_0$ and the maximum $m_{A'} = \sqrt{1+\kappa}m_0$. Thus one can obtain two sets of ϵ^2 constraints as a function of m_0, accordingly. For a given m_0, the best limit usually comes from the maximum, as explained by Eq. (13). Interestingly, one can even constrain m_0 below the dilepton mass threshold via the maximum peak; e.g. the dimuon limit of LHCb extends to m_0 much smaller than $2M_\mu$, as shown in Fig. 2.

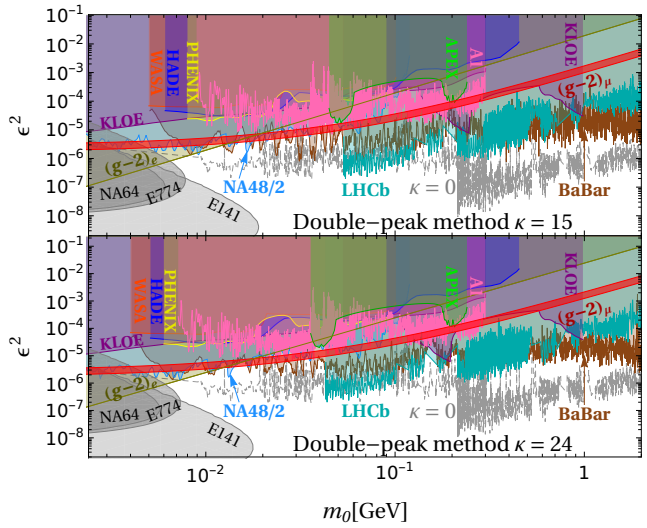

Figure 2. Limits on mixing strength ϵ^2 as a function of mass parameter m_0 using the double-peak method for $\kappa = 15$ and 24, and the traditional limit ($\kappa = 0$) in gray dashed line. The red-shaded region can provide a solution to $(g-2)_\mu$.

Besides Table I, other experiments such as APEX [48], HADES [49], KLOE [50–53], PHENIX [54] and WASA [55], generally provide relatively weaker constraints on ϵ^2 in interested parameter space. Hence, for simplicity we recast their results by rescaling the limits on ϵ according to the time exposure in a bin.

The constraints on our time-varying signal model from above experiments are plotted in Fig. 2. We can see that for $m_0 \gtrsim 10^{-2}$ GeV and $\kappa \sim \mathcal{O}(10)$, current experiments constrain $\epsilon^2 \gtrsim 10^{-7} - 10^{-5}$, around 1 order weaker than the traditional single-peak bounds, whose envelop is shown as gray dashed line labeled as $\kappa = 0$. Especially, the excluded muon g_μ–2 solution becomes viable.

There are beam dump experiments E774 [42], E141 [43] and NA64 [44]. They set limits on $A' \to \ell^+\ell^-$ based on the number of signal event $N(\epsilon, m_{A'})$, for given ϵ and $m_{A'}$. The A' is produced at beam dump and propagates a distance according to its lifetime and decay branching ratios to $\ell^+\ell^-$. We can translate the experiment upper limit on event number of A' decay, e.g. 17 events for E774, to our scenario, by simply time average the signal

events as

$$\frac{1}{\tau}\int_0^\tau N(\epsilon, m_{A'}(t))dt, \tag{16}$$

and compare it with the upper limit as shown in Fig. 2. The detailed estimation of $N(\epsilon, m_{A'})$ is given in the Appendix.

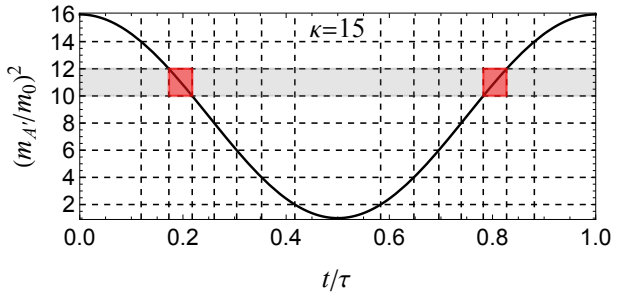

Figure 3. The resonant mass grid can generate the time grid following the signal curve (black). For a fixed row (gray), two particular bins (red) are chosen in the time-dependent method.

V. IMPROVING BY THE TIME-DEPENDENT METHOD

Previous calculations do not exploit the recorded time information of the events and the relevant two parameters are κ and m_0. The experiments can reanalyze the data using both invariant mass and time information, because the signal events only happen at certain time t and mass $m_{A'}(t)$, as shown in Fig. 3. In principle, the experiments can figure out not only κ and m_0 but also m_ϕ and initial phase.

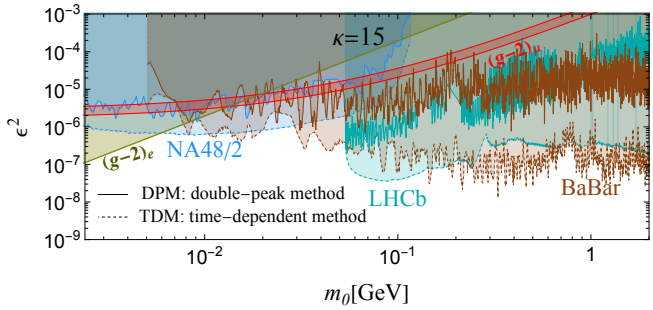

Figure 4. The comparison on mixing strength ϵ^2 between double-peak method and time-dependent method for BaBar [29], LHCb [30–32] and NA48/2 [34].

With no time information in hand, we assume the observed data has a flat probability in time to estimate the signal sensitivity. We adopt the same mass grid as the experiment and it automatically generates the time grid using the signal mass function $m_{A'}(t)$. Specifically, if the total number in the ith mass bin is N_i, we have the number of data in ith mass bin and jth time bin as $N_{i,j} = N_i \Delta t_j/\tau$. For a fixed mass bin (horizontal gray shaded), we pick up the two red bins in Fig. 3, which contain the signal. Adding the data in red bins together, we have

$$N_i^{\rm red} = N_i \frac{1}{\tau}\int_{m_i}^{m_{i+1}} \left|\frac{dt}{dm_{A'}}\right| dm_{A'}, \tag{17}$$

forming a new set of data $N_i^{\rm red}$. Then, our previous calculation using the double-peak method can simply apply.

In this method, the signal event number is unaffected while the background event is suppressed by a factor of $\frac{1}{\tau}\int_{m_i}^{m_{i+1}} \left|\frac{dt}{dm_{A'}}\right| dm_{A'}$. Fig. 4 shows the projected sensitivities using time-dependent analysis for NA48/2, BaBar, and LHCb as examples. Indeed it improves the limits compared with the double-peak method by 1–2 orders of magnitude. The smaller the invariant mass resolution is, the larger improvement is. However, if the mass bin is too small, the analysis will suffer from the statistic error due to small $N_i^{\rm red}$.

VI. INVISIBLE DARK PHOTON

Due to small $g'Q_\phi$, the dominant decay channels of A' are SM fermions. However, it is possible that A' decays to invisible particles dominantly. It has been searched by several experiments including BaBar [56], BES-III [57], NA64 [58] and NA62 [59]. We will briefly discuss how time-varying scenario can affect the results. BaBar and BES-III have studied the monophoton channel, $e^+e^- \to A'\gamma$ with invisible A'. The photon energy is $E_\gamma = (s - m_{A'}^2)/(2\sqrt{s})$ with $\sqrt{s}$ being total collision energy. With time-varying $m_{A'}(t)$, E_γ extends to a spectrum determined by the following differential,

$$\left|\frac{dt}{dE_\gamma}\right| = \frac{\tau}{\pi\sqrt{(E_\gamma - E_{\rm min})\,(E_{\rm max} - E_\gamma)}}, \tag{18}$$

where $E_{\rm min} \equiv (s - (1+\kappa)m_0^2)/(2\sqrt{s})$ and $E_{\rm max} \equiv (s - m_0^2)/(2\sqrt{s})$. Then, the analysis is similar as visible A', by substituting invariant mass bin to photon energy bin and it is expected to weaken the limit. The exception happens for very small m_0 satisfying $m_0^2 < 2\sqrt{s}\sigma_\gamma/\kappa$, with σ_γ being the photon energy resolution. In this case, the limit will be unchanged because both $E_{\rm min}$ and $E_{\rm max}$ fall into the same photon energy bin.

The electron beam dump experiment NA64 [58] studies the process $e^- Z \to e^- Z A'$ for invisible A'. The signal events are selected with $E_{\rm miss} > 50$ GeV and other cuts on electromagnetic and hadronic calorimeter energies. Since $E_{\rm miss}$ is much larger than interested $m_{A'}$, the cut efficiency should not significantly depend on $m_{A'}$. Therefore, the dominant effect of time-varying $m_{A'}$ will show up in the production rate, scaling as $m_e^2/m_{A'}^2$ [46]. Thus one can take the time average for this factor to

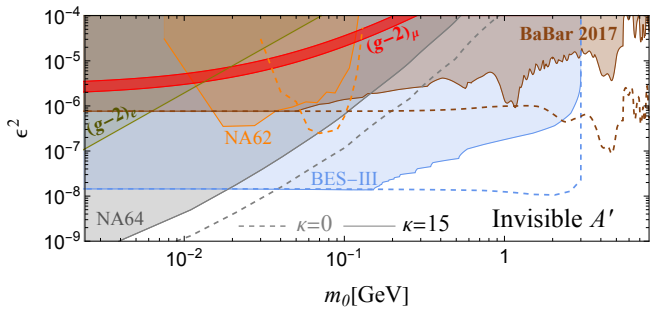

Figure 5. Limits on mixing strength ϵ^2 as a function of mass parameter m_0 using the double-peak method for $\kappa = 15$ for invisible dark photon searches (BaBar [56], BES-III [57], NA64 [58] and NA62 [59]).

estimate the weakening of the limits. Another beam dump experiment NA62 [59] focuses on invisible A' from $\pi^0 \to \gamma A'$, where A' mass is reconstructed using the process $K^\pm \to \pi^\pm \pi^0$ as $m^2_{\rm res} = (p_{K^\pm} - p_{\pi^\pm} - p_\gamma)^2$. One can use double-peak method to analyze the data and set the new limits.

The results are shown in Fig. 5, in which the $(g-2)_\mu$ parameter space has been fully excluded, even for the time-varying signal. To have a dark photon $(g-2)_\mu$ solution, we shall assume the invisible decay channel is subdominant.

VII. OTHER CONSTRAINTS

Besides collider and beam dump experiments, there are other constraints to clarify. Firstly, the coupling $g'Q_\phi$ should be small to avoid ϕ thermalization via self-scattering and scattering with normal matter via $f\phi \to f\phi$ or $f\bar{f} \leftrightarrow \phi\phi^*$. Secondly, the $A' \to \phi\phi^*$ decay could freeze-in ϕ as a hot relic, which should be very small. For interested parameter space $m_0 \sim \mathcal{O}(0.1)$ GeV, the coupling $g'Q_\phi$ around 10^{-6}–10^{-10}, is small enough to satisfy the above requirements for $m_\phi \sim 10^{-20}$–10^{-17} eV, while keeping $\kappa \sim \mathcal{O}(10)$. Moreover, in the early Universe, the field value of ϕ is much larger than today. Thus, a heavy A' mass helps to evade the thermalization and freeze-in constraints. For ultralight scalar, the black hole superradiance can exclude some mass regions but not all the interested regions [60, 61].

At 1-loop level, the SM fermion mass can receive a QED-like correction from A' interaction,

$$\frac{\Delta m_f}{m_f} \simeq \frac{3\left(e\epsilon Q_f\right)^2}{16\pi^2} \log\left(\frac{m_0^2 + 2(g'Q_\phi)^2\phi^*\phi}{m_0^2}\right),$$

with $m_{A'} \gg m_f$. This leads to a logarithmic coupling between $(\phi^*\phi)$ and fermion mass operator, and its Taylor expansion can not be naively truncated due to large κ, hence is totally different with the linear and quadratic couplings. Especially, for these experiments relying on certain ϕ field distribution around massive objects, such as Cassini stochastic, binary pulsars tests [62, 63], atomic clocks [64, 65], torsion balances [66–68], and MICROSCOPE space experiment [69], their constraints do not apply. As for the traditional fifth force experiments [70, 71], even for the quadratic coupling, it only provides a loose bound [11, 72], which can be easily satisfied for small ϵ and $g'Q_\phi$. The constraints from Big Bang nucleosynthesis due to the enhanced ϕ value [11, 73], can be easily evaded in our scenario thanks to the logarithmic coupling.

VIII. CONCLUSION

We have introduced time-varying resonant mass and found it can lead to *double-peak* feature in the invariant mass spectrum, which can help to evade the dilepton and missing mass resonant searches at collider and beam dump experiments. Moreover, the mass spectrum is independent of time if the experiments last longer than the oscillation period. A concrete model is discussed with ultralight complex scalar DM inducing an oscillating mass for kinetic mixing dark photon. For mass around tens of MeV, the already excluded muon $(g-2)_\mu$ solution from A' becomes viable again, and it can be further tested by reanalyzing the existing data with timing information.

ACKNOWLEDGMENTS

Acknowledgments– We would like to thank Maxim Pospelov and Wei Xue for useful discussions, and Bertrand Echenard for helpful discussion on BaBar's data and analysis. JL is supported by the National Science Foundation of China under Grant No. 12075005 and by Peking University under startup Grant No. 7101502458. XPW is supported by the National Science Foundation of China under Grant No. 12005009. KPX is supported by the National Science Foundation under grant number PHY-1820891, and PHY-2112680, and the University of Nebraska Foundation.

Appendix A: Appendix

We show the detailed log-likelihood ratio (LLR) calculations for the collider and beam dump experiments respectively. The recasts are in good agreement with the existing experimental limits, therefore the calculations for time-varying signals are robust.

1. Collider experiments

The BaBar collaboration collected 514 fb^{-1} data at the vicinity of the $\Upsilon(4S)$, $\Upsilon(3S)$ and $\Upsilon(2S)$ resonances

to search for $e^+e^- \to \gamma A'$ process, with $A' \to e^+e^-$ and $\mu^+\mu^-$ decay channels within a mass range 0.02 GeV $< m_{A'} <$ 10.2 GeV [29]. A total of $N_e = 5704$ ($N_\mu = 5370$) mass hypotheses are searched in the e^+e^- ($\mu^+\mu^-$) channel respectively. For a given mass $m_{A'}$, an interval of $m_{A'} \pm 10\,\sigma_{\rm re}$ is used to perform the fits, where $\sigma_{\rm re}$ is the energy resolution at $m_{A'}$, varying from 1.5 to 8 MeV in the whole $m_{A'}$ range. Even though the full data is not given in Ref. [29], there are available data of m_{ee} and $m_R = \sqrt{m_{\mu\mu}^2 - 4M_\mu^2}$ spectrum up to $\sim$ 10 GeV with a uniform bin size of 100 MeV in the main text, and the zoomed in spectrum for $m_{ee} \in [17.8, 62.2]$ MeV ($m_R \in [0.522, 77.4]$ MeV) with a bin size of 0.5 MeV (1.0 MeV) in the supplemental material. We refer the former and latter as the low- and high-granularity datasets, respectively.

To recast the BaBar results, we first generate the artificial high-granularity data for the whole mass spectrum. For $m_{ee} < 62.2$ MeV ($m_R < 77.4$ MeV), we adopt the high-granularity data themselves; while for higher mass, we use the interpolation of the low-granularity data, including appropriate statistical smearing. We assume the bin size increases linearly with resonant mass and keep the total number of the data to be N_e (N_μ) respectively. The resolution $\sigma_{\rm re}$ is also assumed to be increasing linearly. Finally, for a given mass point $m_{A'}$, we fit the artificial data in the mass window $m_{A'} \pm 10\,\sigma_{\rm re}$. The LLR is defined as

$$-2\log\left[\frac{\mathrm{Max}_{\vec{a}'}\prod_i \mathcal{N}(B_i - B(m_i,\vec{a}') - S f_G(m_i)|B_i)}{\mathrm{Max}_{\vec{a}}\prod_i \mathcal{N}(B_i - B(m_i,\vec{a})|B_i)}\right], \tag{A1}$$

where B_i is the background event number in the ith mass bin, and

$$B(m_i,\vec{a}) = a_0 + a_1 m_i + a_2 m_i^2, \tag{A2}$$

is the background fitting function with m_i being the center value of ith bin for m_{ee} or m_R, while

$$\mathcal{N}(x|\sigma^2) \equiv \frac{1}{\sqrt{2\pi}\sigma}\exp\left\{-\frac{x^2}{2\sigma^2}\right\}, \tag{A3}$$

is the normalized Gaussian distribution and S is the total signal event number. $f_G(m_i)$ is the signal template without the time-varying effect, and after detector smearing it is defined as

$$f_G(m_i) = \mathcal{N}(m_{A'} - m_i|\sigma_{\rm re}^2). \tag{A4}$$

It is worth mentioning that in the LLR calculation only statistical error is considered and there is an extra Jacobi factor for the dimuon channel from the definition of m_R.

After requiring LLR = 3.84, we obtain the limits on the allowed signal total event S. They can be used to unfold the limit on $\sigma(e^+e^- \to \gamma A')$ via the acceptance factor 0.15 (0.35) in the dielectron (dimuon) channel respectively [29]. We found our simulated results are consistent with BaBar's results as shown in Fig. 6 for both

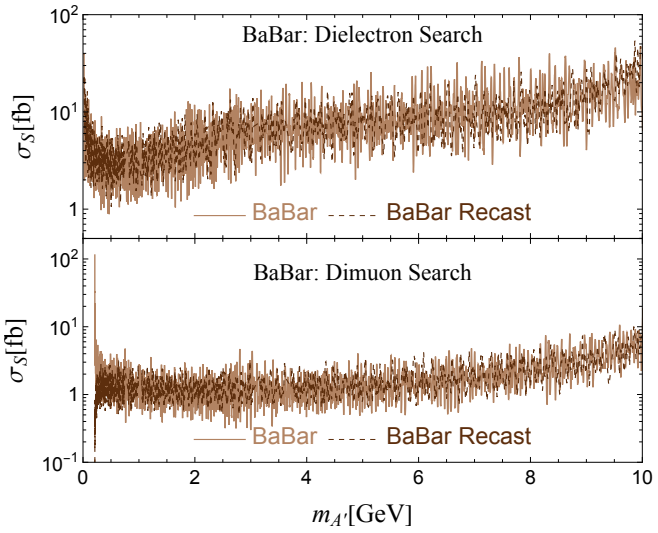

Figure 6. The upper limit on signal cross-section without the time-varying effect, as a function of $m_{A'}$ in dielectron (up) and dimuon (down) channels for BaBar, where the existing and recasted limits are plotted as solid and dashed lines respectively.

e^+e^- and $\mu^+\mu^-$ channels. Therefore, our artificial data and LLR calculation are robust.

Returning to the time-varying scenario, the signal invariant mass spectrum follows the probability density function $f(y)$ in the main text, with $y = m_{\rm res}/m_0$. Adding the smearing effect, the signal template becomes

$$f_S(m_i) = \int_{m_{\rm min}}^{m_{\rm max}} f\left(\frac{m'}{m_0}\right)\mathcal{N}(m_i - m'|\sigma_{\rm re}^2)dm', \tag{A5}$$

with $m_{\rm min} = m_0$ and $m_{\rm max} = \sqrt{1+\kappa}m_0$. In the dimuon channel, the additional Jacobi factor should be taken into account as m_i refers to m_R not $m_{\mu\mu}$. The time-varying scenario is then fitted by using f_S in Eq. (A1) instead of f_G. As f_S peaks around $m_{\rm min}$ and $m_{\rm max}$, for a given $m_{A'}$ we perform two independent fits for $m_0 = m_{A'}$ and $m_0 = m_{A'}/\sqrt{1+\kappa}$ respectively. Therefore, given a $m_{A'}$ we can obtain two sets of limits on the allowed S corresponding to left and right peaks respectively.

To reduce the systematic uncertainties, we take the ratio of S from the time-varying resonant mass scenario f_S and the single mass f_G, to rescale the ϵ^2 constraints from the BaBar measurement [29]. Then, we obtain two sets of ϵ^2 limits as functions of $m_{A'}$, for $m_0 = m_{A'}$ and $m_0 = m_{A'}/\sqrt{1+\kappa}$ respectively, and for each flavor channel. They can be translated to ϵ^2 limits as a function of m_0. Since the right peak of f_S is usually higher than the left peak, for a given m_0, the most stringent constraint usually comes from the mass window around $m_{A'} = \sqrt{1+\kappa}m_0$. This is adopted as the BaBar constraints on our time-varying resonance scenario.

A similar strategy is applied to recast and reinterpret the LHCb measurements in the $pp \to A' \to \mu^+\mu^-$ channel, with an integrated luminosity of ~ 5 fb^{-1}. We take

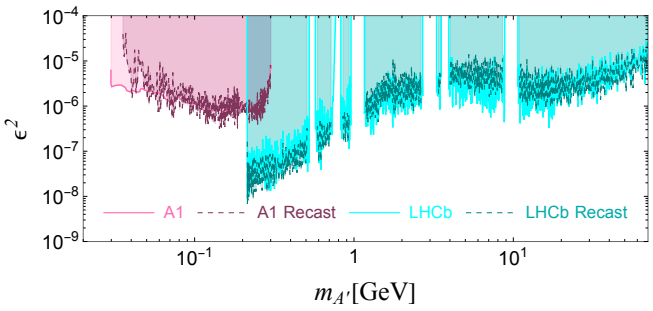

Figure 7. Limits on mixing strength ϵ^2 as a function of mass parameter $m_{A'}$ in A1 and LHCb without the time-varying effect, where the existing and recasted limits are drawn as solid and dashed respectively.

the $m_{\mu\mu}$ data from Ref. [32], and use the method described in Ref. [31] to fit the data and obtain the allowed signal event S. Fortunately, the $n_{\rm ex}^{A'}[m_{A'}, \epsilon^2]/\epsilon^2$ spectrum is provided in the supplementary material of Ref. [31], which contains the signal efficiency to unfold the limit on S to ϵ^2. Assuming the Gaussian smearing of the signal, we have perfectly repeated the LHCb constraints as shown in Fig. 7. Again, we replace f_G with f_S to obtain the bounds for the time-varying scenario. Similar to the BaBar experiment, for each $m_{A'}$ we perform two fits for the double peaks respectively. They can be translated to ϵ^2 limits as a function of m_0 for the LHCb experiment.

An analogous procedure is performed to A1 experiment in the fixed-target electron scattering process $e^- Z \to e^- Z A'$, $A' \to e^+ e^-$ for 0.040 GeV $\lesssim m_{A'} \lesssim$ 0.300 GeV in 2014 [33]. With the data taken from Ref. [33], the well consistent exclusion limits are recasted with the Gaussian smeared signal, as shown in Fig. 7. Similar to BaBar and LHCb experiment, the double-peak method is once again applied to obtain new limits on ϵ^2 as a function of m_0.

2. Beam dump experiments

The beam dump experiments E774 [42], E141 [43] and NA64 [44], are all electron fixed-target experiments. The dark photon A' are dominantly produced by electron Bremsstrahlung process, $e^- Z \to e^- Z A'$ [45, 46]. The A' will travel some distance and decay before reaching the detector. Since there is shielding behind the collision target, A' must have a lifetime with macroscopic scale. To simplify our analysis, we employ the estimate of the A' signal event number following Refs. [25, 45–47],

$$N(\epsilon, m_{A'}) = N_e \mathcal{C}' \epsilon^2 \frac{m_e^2}{m_{A'}^2} e^{-a_1 L_{\rm sh} \Gamma_{A'}} (1 - e^{-a_2 L_{\rm dec} \Gamma_{A'}}), \tag{A6}$$

where N_e is the total electron number in experiments, $\mathcal{C}'$ is a parameter defined in Ref. [46] with typical value of 10, a_1 and a_2 are fitting parameters, $\Gamma_{A'}$ is the decay width of A', $L_{\rm sh}$ is the distance of the end of the shield and $L_{\rm dec}$ is the distance of detector from the collision point. The constraints are obtained by requiring $N(\epsilon, m_{A'})$ equal to the allowed signal events, for example 17 events for E774. We adjust the fitting parameter a_1 and a_2 to reproduce the original results from the experiments. The results are shown in Fig. 8 and one can see the fits are quite well.

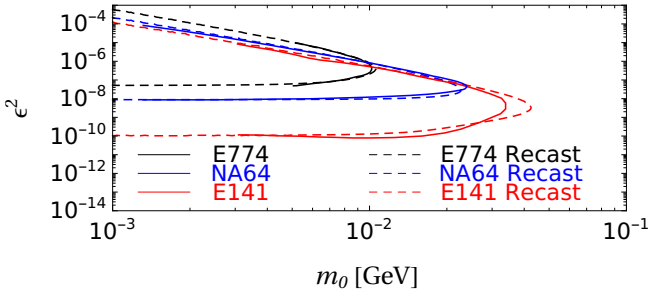

Figure 8. The constraints of beam dump experiments obtained from our estimation Eq. (A6) are shown in solid lines, comparing with corresponding results obtained from experiments and early analysis shown in dashed lines.

Then, with the obtained $a_{1,2}$ we constrain the time-varying scenario by replacing $N(\epsilon, m_{A'})$ with its time average, namely

$$\begin{aligned} N(\epsilon, m_0, \kappa) &= \frac{1}{t_{\rm exp}} \int N(\epsilon, m_{A'}(t)) dt \\ &= \frac{1}{\tau} \int_{m_0}^{\sqrt{1+\kappa} m_0} N(\epsilon, m_{A'}) \left| \frac{dt}{dm_{A'}} \right| dm_{A'}. \end{aligned} \tag{A7}$$

Finally, setting $N(\epsilon, m_0, \kappa)$ to the allowed signal events, we obtain the limits for the time-varying scenario.

[1] P. A. M. Dirac, "The Cosmological constants," Nature **139** (1937) 323.

[2] J.-P. Uzan, "The Fundamental Constants and Their Variation: Observational Status and Theoretical Motivations," Rev. Mod. Phys. **75** (2003) 403, arXiv:hep-ph/0205340.

[3] V. V. Flambaum, "Variation of fundamental constants in space and time: Theory and observations," Eur. Phys. J. ST **163** (2008) 159–171, arXiv:0801.1994 [nucl-th].

[4] T. Dent, "Fundamental constants and their variability in theories of High Energy Physics," Eur. Phys. J. ST **163** (2008) 297–313, arXiv:0802.1725 [hep-ph].

[5] J.-P. Uzan, "Varying Constants, Gravitation and Cosmology," Living Rev. Rel. **14** (2011) 2, arXiv:1009.5514 [astro-ph.CO].

[6] M. Battaglieri et al., "US Cosmic Visions: New Ideas in Dark Matter 2017: Community Report," in U.S. Cosmic Visions: New Ideas in Dark Matter. 7, 2017. arXiv:1707.04591 [hep-ph].

[7] D. Kimball and e. K. van Bibber, The Search for Ultralight Bosonic Dark Matter. Springer, 2022.

[8] D. Antypas et al., "New Horizons: Scalar and Vector Ultralight Dark Matter," arXiv:2203.14915 [hep-ex].

[9] A. Arvanitaki, J. Huang, and K. Van Tilburg, "Searching for dilaton dark matter with atomic clocks," Phys. Rev. D **91** no. 1, (2015) 015015, arXiv:1405.2925 [hep-ph].

[10] Y. V. Stadnik and V. V. Flambaum, "Searching for dark matter and variation of fundamental constants with laser and maser interferometry," Phys. Rev. Lett. **114** (2015) 161301, arXiv:1412.7801 [hep-ph].

[11] Y. V. Stadnik and V. V. Flambaum, "Can dark matter induce cosmological evolution of the fundamental constants of Nature?," Phys. Rev. Lett. **115** no. 20, (2015) 201301, arXiv:1503.08540 [astro-ph.CO].

[12] M. Pospelov, S. Pustelny, M. P. Ledbetter, D. F. Jackson Kimball, W. Gawlik, and D. Budker, "Detecting Domain Walls of Axionlike Models Using Terrestrial Experiments," Phys. Rev. Lett. **110** no. 2, (2013) 021803, arXiv:1205.6260 [hep-ph].

[13] A. Derevianko and M. Pospelov, "Hunting for topological dark matter with atomic clocks," Nature Phys. **10** (2014) 933, arXiv:1311.1244 [physics.atom-ph].

[14] Y. V. Stadnik and V. V. Flambaum, "Searches for topological defect dark matter via nongravitational signatures," Phys. Rev. Lett. **113** no. 15, (2014) 151301, arXiv:1405.5337 [hep-ph].

[15] M. S. Safronova, D. Budker, D. DeMille, D. F. J. Kimball, A. Derevianko, and C. W. Clark, "Search for New Physics with Atoms and Molecules," Rev. Mod. Phys. **90** no. 2, (2018) 025008, arXiv:1710.01833 [physics.atom-ph].

[16] D. J. E. Marsh and S. Hoof, "Astrophysical Searches and Constraints on Ultralight Bosonic Dark Matter," arXiv:2106.08797 [hep-ph].

[17] L. B. Okun, "LIMITS OF ELECTRODYNAMICS: PARAPHOTONS?," Sov. Phys. JETP **56** (1982) 502.

[18] P. Galison and A. Manohar, "TWO Z's OR NOT TWO Z's?," Phys. Lett. B **136** (1984) 279–283.

[19] B. Holdom, "Two U(1)'s and Epsilon Charge Shifts," Phys. Lett. B **166** (1986) 196–198.

[20] M. Pospelov, A. Ritz, and M. B. Voloshin, "Secluded WIMP Dark Matter," Phys. Lett. B **662** (2008) 53–61, arXiv:0711.4866 [hep-ph].

[21] N. Arkani-Hamed, D. P. Finkbeiner, T. R. Slatyer, and N. Weiner, "A Theory of Dark Matter," Phys. Rev. D **79** (2009) 015014, arXiv:0810.0713 [hep-ph].

[22] R. Essig et al., "Working Group Report: New Light Weakly Coupled Particles," in Community Summer Study 2013: Snowmass on the Mississippi. 10, 2013. arXiv:1311.0029 [hep-ph].

[23] J. Alexander et al., "Dark Sectors 2016 Workshop: Community Report," 8, 2016. arXiv:1608.08632 [hep-ph].

[24] P. Ilten, Y. Soreq, M. Williams, and W. Xue, "Serendipity in dark photon searches," JHEP **06** (2018) 004, arXiv:1801.04847 [hep-ph].

[25] M. Bauer, P. Foldenauer, and J. Jaeckel, "Hunting All the Hidden Photons," JHEP **07** (2018) 094, arXiv:1803.05466 [hep-ph].

[26] **Muon g-2** Collaboration, G. W. Bennett et al., "Final Report of the Muon E821 Anomalous Magnetic Moment Measurement at BNL," Phys. Rev. D **73** (2006) 072003, arXiv:hep-ex/0602035.

[27] **Muon g-2** Collaboration, B. Abi et al., "Measurement of the Positive Muon Anomalous Magnetic Moment to 0.46 ppm," Phys. Rev. Lett. **126** no. 14, (2021) 141801, arXiv:2104.03281 [hep-ex].

[28] M. Pospelov, "Secluded U(1) below the weak scale," Phys. Rev. D **80** (2009) 095002, arXiv:0811.1030 [hep-ph].

[29] **BaBar** Collaboration, J. P. Lees et al., "Search for a Dark Photon in e^+e^- Collisions at BaBar," Phys. Rev. Lett. **113** no. 20, (2014) 201801, arXiv:1406.2980 [hep-ex].

[30] **LHCb** Collaboration, R. Aaij et al., "Search for Dark Photons Produced in 13 TeV pp Collisions," Phys. Rev. Lett. **120** no. 6, (2018) 061801, arXiv:1710.02867 [hep-ex].

[31] **LHCb** Collaboration, R. Aaij et al., "Search for $A' \to \mu^+\mu^-$ Decays," Phys. Rev. Lett. **124** no. 4, (2020) 041801, arXiv:1910.06926 [hep-ex].

[32] **LHCb** Collaboration, R. Aaij et al., "Searches for low-mass dimuon resonances," JHEP **10** (2020) 156, arXiv:2007.03923 [hep-ex].

[33] H. Merkel et al., "Search at the Mainz Microtron for Light Massive Gauge Bosons Relevant for the Muon g-2 Anomaly," Phys. Rev. Lett. **112** no. 22, (2014) 221802, arXiv:1404.5502 [hep-ex].

[34] **NA48/2** Collaboration, J. R. Batley et al., "Search for the dark photon in π^0 decays," Phys. Lett. B **746** (2015) 178–185, arXiv:1504.00607 [hep-ex].

[35] J. Preskill, M. B. Wise, and F. Wilczek, "Cosmology of the Invisible Axion," Phys. Lett. B **120** (1983) 127–132.

[36] L. F. Abbott and P. Sikivie, "A Cosmological Bound on the Invisible Axion," Phys. Lett. B **120** (1983) 133–136.

[37] M. Dine and W. Fischler, "The Not So Harmless Axion," Phys. Lett. B **120** (1983) 137–141.

[38] D. J. E. Marsh, "Axion Cosmology," Phys. Rept. **643** (2016) 1–79, arXiv:1510.07633 [astro-ph.CO].

[39] K. K. Rogers and H. V. Peiris, "Strong Bound on Canonical Ultralight Axion Dark Matter from the Lyman-Alpha Forest," Phys. Rev. Lett. **126** no. 7, (2021) 071302, arXiv:2007.12705 [astro-ph.CO].

[40] L. Morel, Z. Yao, P. Cladé, and S. Guellati-Khélifa, "Determination of the fine-structure constant with an accuracy of 81 parts per trillion," Nature **588** no. 7836, (2020) 61–65.

[41] G. Cowan, K. Cranmer, E. Gross, and O. Vitells, "Asymptotic formulae for likelihood-based tests of new physics," Eur. Phys. J. C **71** (2011) 1554, arXiv:1007.1727 [physics.data-an]. [Erratum: Eur.Phys.J.C 73, 2501 (2013)].

[42] A. Bross, M. Crisler, S. H. Pordes, J. Volk, S. Errede, and J. Wrbanek, "A Search for Shortlived Particles Produced in an Electron Beam Dump," Phys. Rev. Lett. **67** (1991) 2942–2945.

[43] E. M. Riordan et al., "A Search for Short Lived Axions in an Electron Beam Dump Experiment," Phys. Rev. Lett. **59** (1987) 755.

[44] **NA64** Collaboration, D. Banerjee et al., "Improved limits on a hypothetical X(16.7) boson and a dark

photon decaying into e^+e^- pairs," Phys. Rev. D **101** no. 7, (2020) 071101, arXiv:1912.11389 [hep-ex].

[45] S. Andreas, C. Niebuhr, and A. Ringwald, "New Limits on Hidden Photons from Past Electron Beam Dumps," Phys. Rev. D **86** (2012) 095019, arXiv:1209.6083 [hep-ph].

[46] J. D. Bjorken, R. Essig, P. Schuster, and N. Toro, "New Fixed-Target Experiments to Search for Dark Gauge Forces," Phys. Rev. D **80** (2009) 075018, arXiv:0906.0580 [hep-ph].

[47] J. Liu, N. McGinnis, C. E. M. Wagner, and X.-P. Wang, "A light scalar explanation of $(g-2)_\mu$ and the KOTO anomaly," JHEP **04** (2020) 197, arXiv:2001.06522 [hep-ph].

[48] **APEX** Collaboration, S. Abrahamyan et al., "Search for a New Gauge Boson in Electron-Nucleus Fixed-Target Scattering by the APEX Experiment," Phys. Rev. Lett. **107** (2011) 191804, arXiv:1108.2750 [hep-ex].

[49] **HADES** Collaboration, G. Agakishiev et al., "Searching a Dark Photon with HADES," Phys. Lett. B **731** (2014) 265–271, arXiv:1311.0216 [hep-ex].

[50] **KLOE-2** Collaboration, A. Anastasi et al., "Limit on the production of a new vector boson in $e^+e^- \to U\gamma$, $U \to \pi^+\pi^-$ with the KLOE experiment," Phys. Lett. B **757** (2016) 356–361, arXiv:1603.06086 [hep-ex].

[51] A. Anastasi et al., "Limit on the production of a low-mass vector boson in $e^+e^- \to U\gamma$, $U \to e^+e^-$ with the KLOE experiment," Phys. Lett. B **750** (2015) 633–637, arXiv:1509.00740 [hep-ex].

[52] **KLOE-2** Collaboration, D. Babusci et al., "Search for light vector boson production in $e^+e^- \to \mu^+\mu^-\gamma$ interactions with the KLOE experiment," Phys. Lett. B **736** (2014) 459–464, arXiv:1404.7772 [hep-ex].

[53] **KLOE-2** Collaboration, D. Babusci et al., "Limit on the production of a light vector gauge boson in phi meson decays with the KLOE detector," Phys. Lett. B **720** (2013) 111–115, arXiv:1210.3927 [hep-ex].

[54] **PHENIX** Collaboration, A. Adare et al., "Search for dark photons from neutral meson decays in $p+p$ and d + Au collisions at $\sqrt{s_{NN}} = 200$ GeV," Phys. Rev. C **91** no. 3, (2015) 031901, arXiv:1409.0851 [nucl-ex].

[55] **WASA-at-COSY** Collaboration, P. Adlarson et al., "Search for a dark photon in the $\pi^0 \to e^+e^-\gamma$ decay," Phys. Lett. B **726** (2013) 187–193, arXiv:1304.0671 [hep-ex].

[56] **BaBar** Collaboration, J. P. Lees et al., "Search for Invisible Decays of a Dark Photon Produced in e^+e^- Collisions at BaBar," Phys. Rev. Lett. **119** no. 13, (2017) 131804, arXiv:1702.03327 [hep-ex].

[57] Y. Zhang, W.-T. Zhang, M. Song, X.-A. Pan, Z.-M. Niu, and G. Li, "Probing invisible decay of dark photon at BESIII and future STCF via monophoton searches," Phys. Rev. D **100** no. 11, (2019) 115016, arXiv:1907.07046 [hep-ph].

[58] D. Banerjee et al., "Dark matter search in missing energy events with NA64," Phys. Rev. Lett. **123** no. 12, (2019) 121801, arXiv:1906.00176 [hep-ex].

[59] **NA62** Collaboration, E. Cortina Gil et al., "Search for production of an invisible dark photon in π^0 decays," JHEP **05** (2019) 182, arXiv:1903.08767 [hep-ex].

[60] A. Arvanitaki, M. Baryakhtar, and X. Huang, "Discovering the QCD Axion with Black Holes and Gravitational Waves," Phys. Rev. D **91** no. 8, (2015) 084011, arXiv:1411.2263 [hep-ph].

[61] H. Davoudiasl and P. B. Denton, "Ultralight Boson Dark Matter and Event Horizon Telescope Observations of M87*," Phys. Rev. Lett. **123** no. 2, (2019) 021102, arXiv:1904.09242 [astro-ph.CO].

[62] J. W. Armstrong, L. Iess, P. Tortora, and B. Bertotti, "Stochastic gravitational wave background: Upper limits in the 10**-6-Hz 10**-3-Hz band," Astrophys. J. **599** (2003) 806–813.

[63] D. Blas, D. L. Nacir, and S. Sibiryakov, "Ultralight Dark Matter Resonates with Binary Pulsars," Phys. Rev. Lett. **118** no. 26, (2017) 261102, arXiv:1612.06789 [hep-ph].

[64] K. Van Tilburg, N. Leefer, L. Bougas, and D. Budker, "Search for ultralight scalar dark matter with atomic spectroscopy," Phys. Rev. Lett. **115** no. 1, (2015) 011802, arXiv:1503.06886 [physics.atom-ph].

[65] A. Hees, J. Guéna, M. Abgrall, S. Bize, and P. Wolf, "Searching for an oscillating massive scalar field as a dark matter candidate using atomic hyperfine frequency comparisons," Phys. Rev. Lett. **117** no. 6, (2016) 061301, arXiv:1604.08514 [gr-qc].

[66] G. L. Smith, C. D. Hoyle, J. H. Gundlach, E. G. Adelberger, B. R. Heckel, and H. E. Swanson, "Short range tests of the equivalence principle," Phys. Rev. D **61** (2000) 022001.

[67] S. Schlamminger, K. Y. Choi, T. A. Wagner, J. H. Gundlach, and E. G. Adelberger, "Test of the equivalence principle using a rotating torsion balance," Phys. Rev. Lett. **100** (2008) 041101, arXiv:0712.0607 [gr-qc].

[68] T. A. Wagner, S. Schlamminger, J. H. Gundlach, and E. G. Adelberger, "Torsion-balance tests of the weak equivalence principle," Class. Quant. Grav. **29** (2012) 184002, arXiv:1207.2442 [gr-qc].

[69] P. Touboul et al., "MICROSCOPE Mission: First Results of a Space Test of the Equivalence Principle," Phys. Rev. Lett. **119** no. 23, (2017) 231101, arXiv:1712.01176 [astro-ph.IM].

[70] E. G. Adelberger, B. R. Heckel, S. A. Hoedl, C. D. Hoyle, D. J. Kapner, and A. Upadhye, "Particle Physics Implications of a Recent Test of the Gravitational Inverse Sqaure Law," Phys. Rev. Lett. **98** (2007) 131104, arXiv:hep-ph/0611223.

[71] D. J. Kapner, T. S. Cook, E. G. Adelberger, J. H. Gundlach, B. R. Heckel, C. D. Hoyle, and H. E. Swanson, "Tests of the gravitational inverse-square law below the dark-energy length scale," Phys. Rev. Lett. **98** (2007) 021101, arXiv:hep-ph/0611184.

[72] K. A. Olive and M. Pospelov, "Environmental dependence of masses and coupling constants," Phys. Rev. D **77** (2008) 043524, arXiv:0709.3825 [hep-ph].

[73] S. Sibiryakov, P. Sørensen, and T.-T. Yu, "BBN constraints on universally-coupled ultralight scalar dark matter," JHEP **12** (2020) 075, arXiv:2006.04820 [hep-ph].